PRAMANA
—journal of
physics

Vol. 53, No. 1,
July 1999
pp. 171–197

Structure and dynamics of charged macromolecules: Minimal representation of biological systems

M MUTHUKUMAR
Polymer Science and Engineering Department and Materials Research Science and Engineering Center, University of Massachusetts, Amherst, MA 01003, USA

Abstract. Structures and functions of various biological macromolecules at cellular levels are controlled by electrostatic, excluded-volume, macromolecular topological connectivity, and hydrodynamic forces. Some aspects of these challenging issues will be addressed. Specifically we will focus our discussions on (a) pattern recognition by macromolecules and complexation, (b) coupling between conformational transitions and phase transitions, (c) chromosomal condensation, (d) collective behavior of charged macromolecules in crowded environments, (e) coupled dynamics of macromolecular assemblies in charged solutions, and (f) polymer transport through pores. Even the simpler synthetic systems exhibit many puzzles which will be resolved using our theoretical formulation. In addition to exploring an understanding of biological processes, the context of fabrication of new synthetic materials will be remarked.

Keywords. Charged macromolecules; biological systems; pattern recognition.

PACS Nos 61.25. Hq.; 87.15.-v

1. Introduction

The organization of self-assembled macromolecules and the controlled exhibition of myriads of their functions in natural environments of eucaryotic cells are so complex that traditional tools of theoretical physics might be argued not to be appropriate to understand cell biology. Nevertheless, almost all biological phenomena involve a heirarchy of length and time scales. In this heirarchy, there are certainly large scale structures which are large enough to be treated by statistical mechanics while the details at short scales need to be properly parametrized. Indeed synthetic polymers, while being far simpler than biological macromolecules, have been successfully treated by a variety of statistical mechanics methods for their large scale behavior by surrogating local details in terms of well-calibrated parameters. I believe that a similar advance is in the making for biological assemblies as well. It is in this spirit, I introduce six problems below after briefly mentioning the biological context. The gap between the results of the problems discussed below and the actual biological functions of eucaryotic cells is indeed very wide. But I believe the problems introduced below are necessary basic steps that must be taken before we can hope to understand the large scale behavior of biological systems.

A typical cartoon of a mammalian cell is presented in figure 1. The actual details can be found in any textbook on biology. The noteworthy features for the present discussion are the following. A cell is a very crowded environment consisting of several partitions,

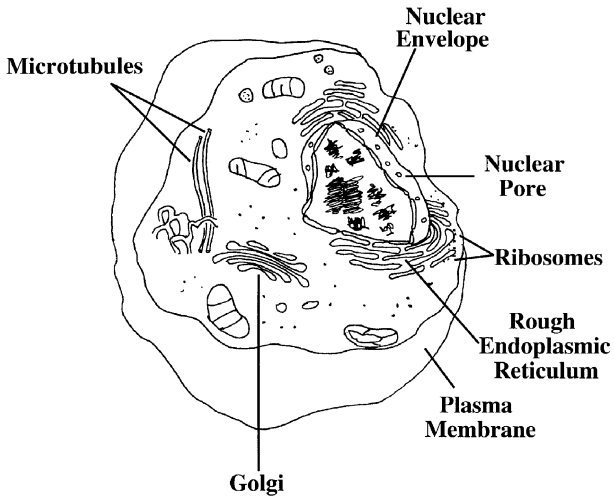

Figure 1. A cell is compartmentalized and crowded.

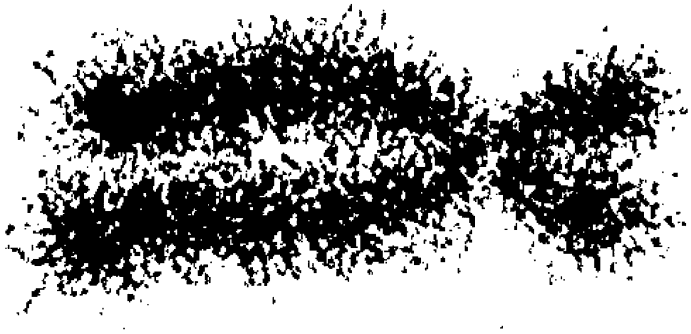

Figure 2. Mitotic chromosome as a compact super complex of DNA and proteins.

each with carefully regulated distributions of macromolecules with prescribed sequences of various monomers. Almost all of these macromolecules are charged and are present in an electrolytic medium with many kinds of small dissociated ions. The cell may be considered to be a crowded 'Coulomb soup'. The charged macromolecules (called polyelectrolytes) physically assemble to form various large structures. For example, the microtubules are self-assembled (i.e., 'polymerized' via noncovalent physical association) structures of thousands of tubulin monomers (themselves being polymers) using a combination of hydrophobic and electrostatic interactions. Another example is the chromosome which is a super complex between the negatively charged DNA and many proteins carrying a net positive charge. The rich heirarchy of structures in the self-assembly of chromosomes are nicely documented in many textbooks [1, 2] on biology. So we only mention here that during the *M*-phase of the cell cycle, the chromosome is a compact complex (figure 2) of very many loops of chromatin fiber (itself being a complex of DNA and proteins) stitched along the chromosomal axis using the so called

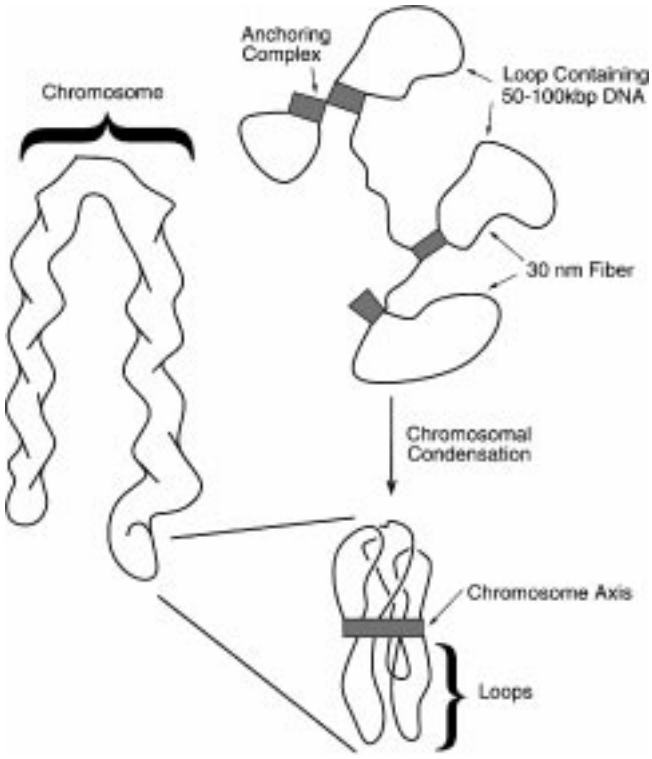

Figure 3. A proposed mechanism for chromosomal condensation.

anchoring complexes. It is to be noted that the loop length is much longer than the persistence length of the fiber. These compactly arranged loops are distributed into the euchromatin and heterochromatin in the *I*-phase which is of the longest duration in the cell cycle. After copying of information contained in the chromosome is completed, the loops are faithfully repackaged back into the *M*-phase chromosome. It is empirically known that the inner membrane of the nuclear envelope plays a crucial role in the distribution and redistribution of DNA loops via many complexation processes. A proposed mechanism for the distribution of loops and the chromosomal condensation is presented in figure 3.

The transport of biological macromolecules under crowded environments is known to occur very effectively from one specific location to another using many signaling methods. For example, proteins synthesized in the proximity of endoplasmic reticulum are transported to the Golgi apparatus, where they undergo modifications and sorting and then they get dispatched to their final destinations. Furthermore the transport of macromolecules is carried out through narrow pores. For example, the *m*-RNA is transported from the nucleus into the cytoplasm through nuclear pores. This is a necessary step before proteins are synthesized which in turn get into the nucleus to control the formation of the *m*-RNA. Therefore it is clear that there is a tremendous amount of cooperativity in various processes involving complexation and transport.

In view of the above basic issues raised in the contexts of biology, we now address the following questions:

1. How do polyelectrolytes complex with oppositely charged objects? The object is either a planar or curved membrane with suitable decoration of patterns of charges.
2. How does the adsorption of a macromolecule to a membrane couple with conformational transitions such as the helix–coil transition? Is there any synergism between adsorption and conformational transitions?
3. How can the chromosomal condensation described in figure 3 be conveniently parametrized?
4. What is the thermodynamic description of a collection of polyelectrolytes in a crowded environment?
5. How do polyelectrolytes move in a concentrated solution? What are the collective effects on chain dynamics?
6. How does a polymer chain escape through a pore?

As mentioned already, it is hoped that answers to these questions will facilitate the exploration of more serious questions related to biological phenomena.

2. Pattern recognition by macromolecules

Recognition of chemical patterns by macromolecules leads to an infinitely diverse set of complexes which results in a wide range of structures, dynamics and functions, as seen overwhelmingly in biological contexts. Only recently have efforts [3] been made to identify the underlying general principles behind pattern recognition in macromolecular self-assembly by studying model systems.

The basic model is sketched in figure 4 where different patterns composed of special chemical groups A are written on a surface and the macromolecule is a two-component linear heteropolymer with segments A^* which are uniquely complementary to A. The A^*

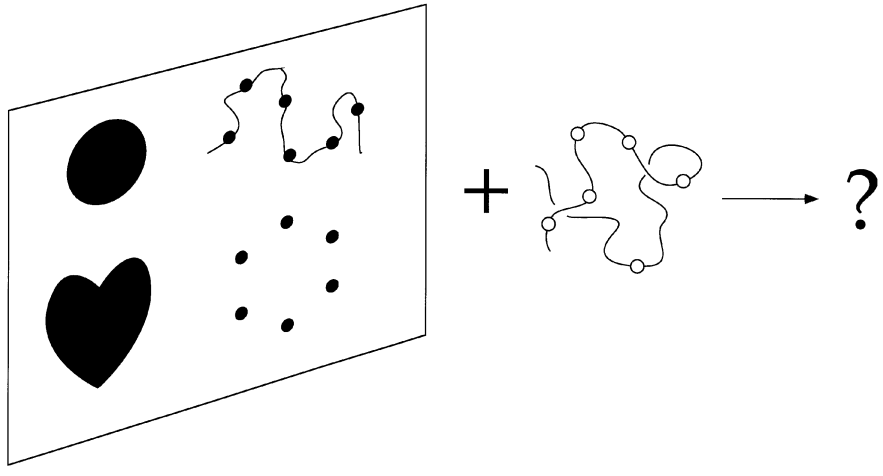

Figure 4. Sketch of a model for pattern recognition.

segments of the polymer are placed on the polymer backbone as a particular sequence. Although the most straightforward approach to this problem is to directly solve a specific example with the appropriate details of the potentials between all pairs of atoms in the system, we ask here whether there are any general principles guiding the pattern recognition process. Specifically we consider the pattern to be made up of electrostatic charges (say +) and the polymer to consist of opposite charges distributed on the chain backbone in a particular sequence. The system is, of course, neutral due to the presence of counter ions. We also consider the presence of salt to modulate the range of the electrostatic interaction. We have chosen the case of polyelectrolytes near a surface with charged patterns as a candidate for the pattern recognition problem due to the nature of the specificity of A (+ve) and A^*(−ve), longer-ranged nature of potential interaction, and the prevalence of such systems in nature.

We represent the polymer chain as a continuous curve [4] and the probability distribution function, $G(\mathbf{R}, \mathbf{R}'; L, 0)$ for the chain of length L to have the ends at $\mathbf{R}$ and $\mathbf{R}'$ is given by the Edwards path integral [5],

$$G(\mathbf{R}, \mathbf{R}'; L, 0) = \int_{\mathbf{R}(0)=\mathbf{R}'}^{\mathbf{R}(L)=\mathbf{R}} \mathcal{D}[\mathbf{R}(s)] \exp\left\{ -\frac{3}{2l} \int_0^L \mathrm{d}s \left(\frac{\partial \mathbf{R}(s)}{\partial s} \right)^2 - \frac{1}{2} \int_0^L \mathrm{d}s \int_0^L \mathrm{d}s' V[\mathbf{R}(s) - \mathbf{R}(s')] - \int_0^L \mathrm{d}s \int \mathrm{d}^2 S V_s(r_s) \right\}. \quad (1)$$

Here $\mathbf{R}(s)$ is the position vector of the arc length variable $s (0 \leq s \leq L)$. l is the Kuhn step length. $L = Nl$, where N is the number of Kuhn segments in a chain. $V(\mathbf{r})$ is the interaction energy between two segments of the chain separated by a distance $\mathbf{r}$,

$$V(\mathbf{r}) = \omega \delta(\mathbf{r}) + l_{\mathrm{B}} q^2 \frac{\mathrm{e}^{-\kappa r}}{r}. \quad (2)$$

ωl^2 is the inter-segment excluded volume arising from the usual short-range interactions. $\delta(\mathbf{r})$ is the Dirac delta function. The second term on the right hand side of eq. (2) describes the screened Coulomb interaction of the Debye–Hückel type. l_{B} is the Bjerrum length,

$$l_{\mathrm{B}} = \frac{e^2}{4\pi \varepsilon_0 \varepsilon_r k_{\mathrm{B}} T}, \quad (3)$$

where e is the electronic charge, ε_0 is the permittivity of vaccuum, ε_r is the dimensionless dielectric constant of the medium bearing the polymer, k_{B} is the Boltzmann constant, and T is the absolute temperature. q is the charge density on the backbone of the chain, charge per Kuhn length. κ is the inverse Debye length, determining the range of the Coulombic interaction. κ^2 is determined by the concentrations of various ions in the system, both the counterions and the ions arising from the presence of any added salt

$$\kappa^2 = 4\pi l_{\mathrm{B}} \sum_i c_i z_i^2, \quad (4)$$

where c_i and z_i are the concentration and valence respectively of the ith ion.

The potential $V_s(r_s)$ of the third term of the exponetial in eq. (1) represents the energy of the electrostatic interaction between a segment and a surface element of area d^2S,

$$V_s(r_s) = -l_B\, \sigma q \frac{e^{-\kappa r_s}}{r_s}. \tag{5}$$

Here r_s is the distance of $\mathbf{R}(s)$ from the center of the surface element and σ is the charge density at the surface element, charge per Kuhn length squared. It is already assumed that the charges on the surface and on the polymer are opposite, due to the minus sign in eq. (5).

The integral equation (1) can be exactly replaced by the differential equation

$$\left[\frac{\partial}{\partial L} - \frac{l}{6}\nabla^2_{\mathbf{R}} + \mathcal{V}(\mathbf{R}) + \mathcal{V}_f(\mathbf{R})\right] G(\mathbf{R}, \mathbf{R}'; L, 0) = 0 \tag{6}$$

with the boundary condition that G vanishes if $\mathbf{R}$ approaches infinity or any part of the surface. The potentials appearing in eq. (6) are given by

$$\mathcal{V}(\mathbf{R}) = \frac{1}{2}\int_0^L ds V[\mathbf{R} - \mathbf{R}(s)] \tag{7}$$

and

$$\mathcal{V}_s(\mathbf{R}) = \int d^2S V_s(r_L), \tag{8}$$

where r_L is the distance of $\mathbf{R}(L)$ from the center of the surface element d^2S.

In its general form, eq. (6) does not allow exact analytical solution. To simplify, we make the assumption that the intrachain excluded volume interactions, both short- and long-ranged, swell the chain uniformly so that the chain can be considered to be an effective Gaussian chain with Kuhn length renormalized into l_1 which is a function of all parameters of the potential V. In spite of the crudeness of this approximation, the size of a polyelectrolyte chain calculated using the uniform expansion approach is in good agreement with both experiments [6] on synthetic polyelctrolytes and simulation results [7]. With this approximation, eq. (6) becomes

$$\left[\frac{\partial}{\partial L} - \frac{l_1}{6}\nabla^2_{\mathbf{R}} + \mathcal{V}_s(\mathbf{R})\right] G(\mathbf{R}, \mathbf{R}'; L, 0) = 0. \tag{9}$$

We now consider the interaction between this effective Gaussian chain and the patterned surface. We illustrate the case of uniformly charged planar surface with charge density σ and merely quote the results for other geometries and patterns. Now $\mathcal{V}_s(\mathbf{R})$ is given by

$$\begin{aligned}\mathcal{V}_s(\mathbf{R}) &= -\int l_B\, \sigma q\, \frac{e^{-\kappa\sqrt{z^2+\rho^2}}}{\sqrt{z^2+\rho^2}} d^2\rho \\ &= -2\pi l_B\, \sigma q\, \frac{e^{-\kappa z}}{\kappa},\end{aligned} \tag{10}$$

where a Cartesian coordinate system is chosen such that the planar surface coincides with the (x, y)-plane. ρ is a vectorial position in the (x, y)-plane. For the particular case of $\mathcal{V}_s$,

eq. (9) separates. G is the product of two functions, one being the solution of a two-dimensional free-diffusion equation and the other for the z-direction. Using the bilinear expansion, we find

$$G(\mathbf{R}, \mathbf{R}'; L, 0) = G(\rho, \rho'; L, 0) \sum_m \psi_m(z)\psi_m(z')\mathrm{e}^{-E_m L}, \tag{11}$$

where ψ_m and E_m are the eigenfunctions and the eigenvalues of

$$\left[-\frac{l_1}{6}\frac{\mathrm{d}^2}{\mathrm{d}z^2} + \mathcal{V}_s(z)\right]\psi_m(z) = E_m\psi_m(z). \tag{12}$$

The eigenvalues and eigenfunctions are to be determined using the boundary condition that $\psi_m(z)$ vanishes on the surface at $z = 0$ and at distances far away from the surface, viz.,

$$\psi_m(0) = 0 = \psi_m(\infty). \tag{13}$$

The separability of eq. (9) occurs only for the special case of eq. (10) and for situations where the patterns on the surface are isotropic. For the case of richer patterns the above separability is not valid and we need to resort to calculations in all dimensions.

Equation (12) is precisely the Schrödinger equation for a particle in an one-dimensional box with the potential energy, $\mathcal{V}_s(z)$. Hence, by drawing the analogy with the quantum-mechanical problem, we expect two regimes with different characteristics. First, for values of $\mathcal{V}_s$ smaller than a certain critical value $\mathcal{V}_{sc}$, to be determined below, the potential has no bound states. Now all E_m are positive and $\psi_m(z)$ will be oscillatory for all z. This corresponds to the state where the polymer is not bound to the pattern. In the second regime, $\mathcal{V}_s > \mathcal{V}_{sc}$, the potential has at least one bound state. This corresponds to the state where the polymer is bound to the pattern.

(i) *Adsorption to a planar surface*

The critical condition for adsorption of a uniformly charged polyelectrolyte to an oppositely and uniformly charged surface is given by

$$\frac{\sigma q l_\mathrm{B}}{\kappa^3 l_1} \geq \frac{0.12}{\pi}. \tag{14}$$

Using the definition of l_B and the expression for l_1, the condition for absorption is given in figure 5 where $4\pi\epsilon\epsilon_0 k_\mathrm{B}T/\sigma q e^2 l^2$ is plotted against κl for $w = 0$ and $N = 60$. In the region below the theoretical curve, there is adsorption. There is no adsorption in the parameter range above the curve. Also the adsorption can be induced by increasing σ, q, or l_B or by decreasing κ. The data points given in the figure are from Monte Carlo simulations [7] for $w = 0$ and $N = 60$, which verify the validity of the assumptions made in the above theoretical calculation.

(ii) *Adsorption to a sphere*

If the adsorbing surface is a sphere of radius R and uniform charge density σ, the critical condition for adsorption is [8]

$$\frac{\sigma q l_\mathrm{B}(1 - \mathrm{e}^{-2\kappa R})}{\kappa^3 l_1} \geq \frac{0.12}{\pi}. \tag{15}$$

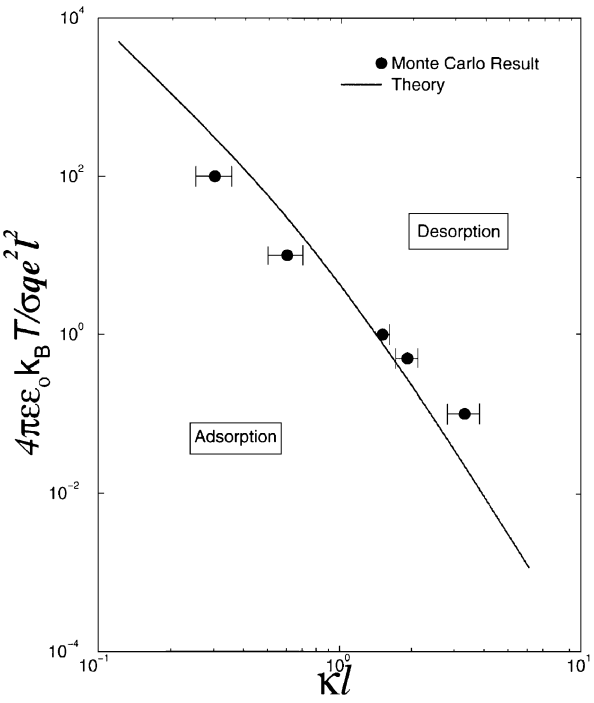

Figure 5. Comparison between eq. (14) and Monte Carlo simulation data.

This expression shows that the sphere radius R can also be used as an additional variable to tune the adsorption. For example, if $\sigma q l_B l^2 = 1$ and $N = 60$, the critical raduis R_c necessary for adsorption is given in figure 6 as a function of κl. In the region above the curve, there is adsorption. The curve is in reasonable agreement with the Monte Carlo data [7] obtained for the same model. It is clear from figure 6 that as the salt concentration increases, increasingly larger spheres desorb.

(iii) *Adsorption to a patterned surface*

Let a pattern of circular symmetry of radius Λ with charge density σ be imprinted on a planar surface to which an oppositely charged polyelectrolyte adsorbs. Now the critical condition for the binding of the polymer to a pattern of size Λ is given by [5]

$$\frac{\sigma q l_B [1 - (\kappa\Lambda + 1)e^{-\kappa\Lambda}]}{\kappa^3 l_1} \geq \frac{0.12}{\pi}. \tag{16}$$

This result is also verified by performing Monte Carlo simulations [5].

(iv) *Complexation between polyions*

The same calculational method used in obtaining the critical condition for binding of a polyelectrolyte to a charged surface can be used to obtain the condition for complexation between a polyanion and a polycation. Two possible situations may be identified. In one

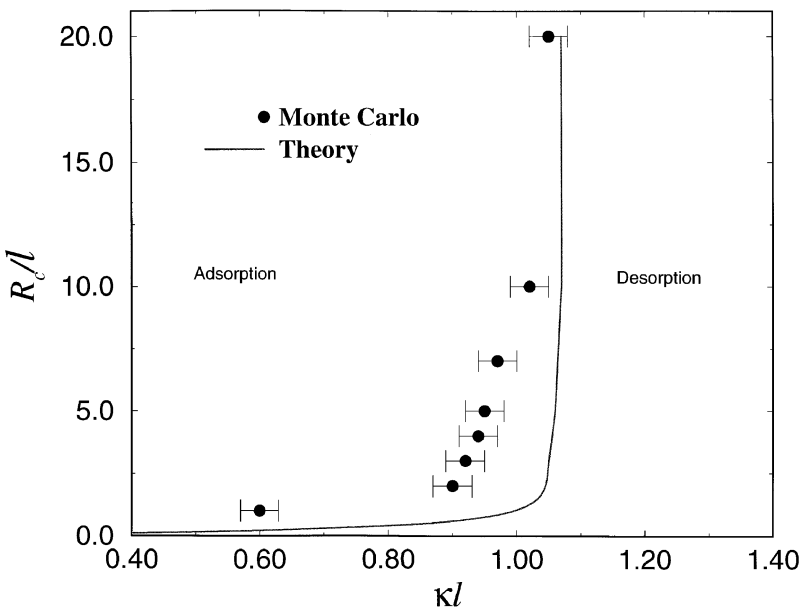

Figure 6. Dependence of critical radius on κ. The curve is eq. (15) and the data are from Monte Carlo simulations.

case, let a mobile polyion with N_2 segments and charge density q_2 complex with a frozen polyion of opposite charge with N_1 segments and charge density q_1. In the second case, let both polyions be mobile. In the first case, the condition for binding at the high salt limit turns out to be

$$\frac{q_1 q_2^{1/5}}{\kappa^{6/5}} \left(\frac{l_B}{l}\right)^{3/5} \frac{N_1}{N_2^{1/5}} \geq A, \tag{17}$$

where A is a constant. It is to be noted that the exponents of N_1 and N_2 are not the same. Similarly the exponents of q_1 and q_2 are different. Thus the frozen host dominates the critical condition for binding over the mobile guest polyion. In the low salt condition, the above condition changes to

$$\left(\frac{q_1^3 l_B l}{q_2}\right)^{1/3} \frac{N_1^3}{N_2} \geq A_1, \tag{18}$$

where A_1 is a constant. Again, the frozen host dominates over the mobile guest. In the second case, where both polyions are mobile, the condition for complexation is determined equally by both chains. For example the radius of gyration of the complex is comparable to that of either chain and is determined by the loop length,

$$R_g \sim R_{g1} \sim R_{g2} \sim \left(\frac{N}{m}\right)^{1/2}, \tag{19}$$

where R_{gi} is the radius of gyration of the ith chain, N is the number of segments in either the polycation or polyanion, and m is the number of pairs that are formed in the complex.

(v) *Kinetics and topological dereliction*

So far we considered only the critical condition for the binding of a polyelectrolyte to an oppositely charged surface (planar or spherical) containing a pattern or another polymer. For the case of polyelectrolytes, the recognition of a specific pattern by a polyelectrolyte with a specific sequence is extremely slow as seen in Monte Carlo simulations. In fact the complexation between two oppositely charged polymers has been seen [9] in Monte Carlo simulations to proceed in two steps. The first step is a relatively fast complexation without registry of the pattern followed by a very slow process of registry.

The inability of a chain to recognize a pattern perfectly in a reasonable time can be understood by the following simple argument. Consider only three units (labelled $i = 1, 2, 3$) making up a linear pattern with a regular spacing b in three dimensional space. Let us proceed to monitor the binding of a portion of a chain with three special segments (labelled $i_p = 1, 2, 3$) complementary to those making up the pattern. Let there be a spacer of $(\mu - 1)$ neutral segments between any two consecutive special segments. Also, let the first special segment be anchored to the end unit of the pattern as shown in figure 7a. Assuming that the chain obeys Gaussian statistics and the gain in energy for contact between any special segment of the polymer and any unit of the pattern is ϵ, the free energy corresponding to the configuration of figure 7a is $-\epsilon$. The second contact between the polymer and the pattern can take place in four possible ways. These are indicated in

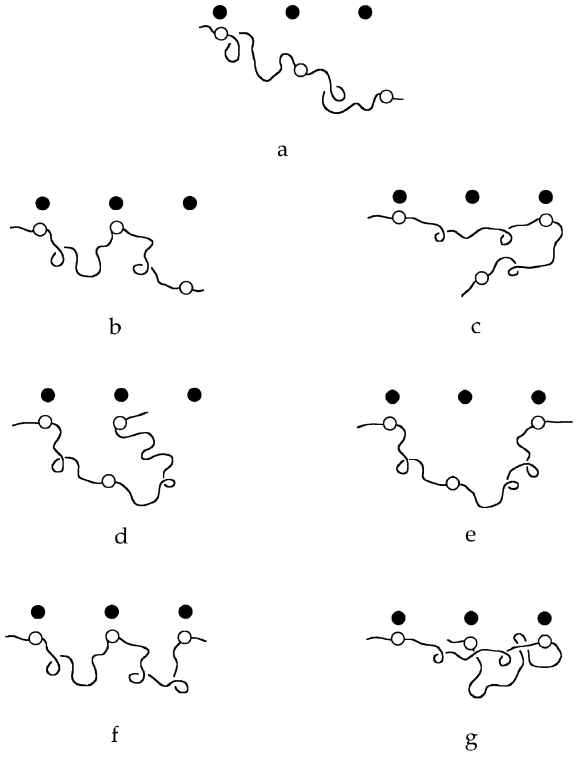

Figure 7. Topological dereliction.

figure 7b–7e. $i_p = 2$ can be paired either with $i = 2$ or 3; $i_p = 3$ can be paired either with $i = 2$ or 3. When $i_p = 2$ is paired with $i = 2$, the end-to-end distance of the polymer spacer with μ segments is b with an accompanying entropic penalty of $s \equiv 3k_B b^2/2\mu l^2$. Therefore the free energy of the complex depicted as the graph of figure 7b is $-2\epsilon + s$ apart from a constant term. Similarly the complexes with contacts $(i_p = 2; i = 3)$, $(i_p = 3; i = 2)$, and $(i_p = 3; i = 3)$ have free energies $-2\epsilon + 4s$, $-2\epsilon + s/2$, and $-2\epsilon + 2s$, respectively. It is to be noted that the complex of figure 7d from $(i_p = 3; i = 2)$ is the most stable complex as far as two-contact complexes are considered and for $b^2/\mu > 2\ln 2$.

Proceeding now to consider the three-contact complexes, there are only two such complexes, as shown in figures 7f and 7g, with respective free energies $-3\epsilon + 2s$ and $-3\epsilon + 5s$. Assuming sequential pairing, the complex with full registry given in figure 7f can arise only from figures 7b and 7e. The complex of figure 7g can arise from figures 7c or 7d. While the most stable complex with only two contacts is that of figure 7d, its further evolution to the three-contact state is to a state with higher free energy and not to the lowest free energy state. It is obvious from the configurations of the complexes shown in figures 7f and 7g, that these configurations cannot be directly converted to each other. The only way the complex of figure 7g can relax to that of figure 7f is to trace its trajectory backwards to its original state and try again to avoid the free energy minimum state at an intermediate time. Thus any effort to minimize the free energy of the system at intermediate times can make the trajectory further away from the proper trajectory leading to the fully registered state of the complex.

The above simple argument illustrates the necessity of optimised temporal correlations for the full pattern recognition. It also indicates that any computational algorithm which minimizes the free energy at every time step can substantially prolong the time needed for full recognition. The same qualitative arguments are valid for the recognition process involving patterns even within a single polymer chain.

The restrictions on the pathways connecting different topological states have two consequences. If k_{ij} is the rate constant for the 'reaction' of going to jth state from ith state, the time dependence of concentration of the system in the ith state is given by

$$\rho(t) = \sum_{\mu=1}^{7} \exp(-t/\tau_\mu), \tag{20}$$

where τ_μ is the relaxation time for the μth normal mode. This result cannot be distinguished from a stretched exponential,

$$\rho(t) \simeq \exp\left[-\left(\frac{t}{\tau}\right)^{\beta}\right], \tag{21}$$

where τ and β are parameters. Since the free energies of the various states are known, the temperature dependence of the entropy S of the system can be calculated. A typical result is given in figure 8 (see ref. [10] for more details). The entropy gradually decreases as the temperature is reduced and then smoothly crosses over to that of a fully registered state without any catastrophy. The stretched exponential nature of time evolution of population and the above mentioned behavior of entropy with respect to temperature are typical properties of glasses. Therefore these glassy features are borne out in the pattern recognition process.

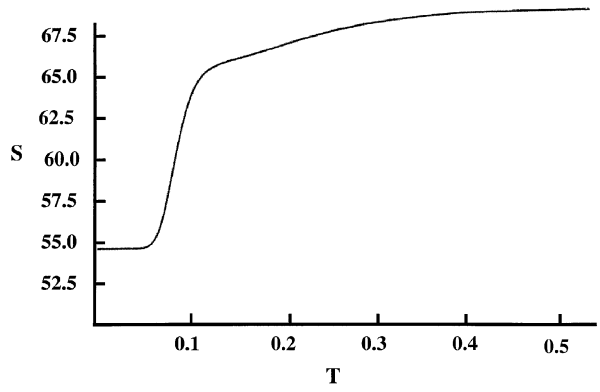

Figure 8. Temperature dependence of entropy for a pattern recognition process.

3. Coupling between adsorption and the helix–coil transition

Many natural and synthetic polymers are known to undergo the conformational transition [11] from a coiled state to a helical state upon lowering the temperature. This conformational transition is not a true thermodynamic phase transition at non-zero temperatures. On the other hand, adsorption [12] of a flexible polymer chain to a planar surface with a short-range attractive potential for polymer segments is a second order phase transition. Using an exactly solvable model [13] we show below that the helix–coil transition gets promoted into a critical phenomenon and the adsorption phase transition is modified into a first order phase transition. We believe that such abrupt changes in polymer conformations due to coupling of two mechanisms are routinely utilized by the biological systems.

It is well known [11] that the helix–coil transition is modeled by mapping into the exactly solvable one-dimensional Ising model. A monomer is either in the coil state or in the helical state. A sample configuration of the polymer chain consists of strings of monomers in the coil state connected continuously by strings of monomers in the helical state. Let $-\epsilon$ be the free energy per segment in the helical state relative to that in the coil state. Let the free energy required to convert the end-helical segment in a string of helical segments to a coil state be $-(1/2)k_{\mathrm{B}}T\ln(\sigma)$. Ignoring non-bonded interactions among segments and using standard methods employed in 1-d Ising model, the fraction of segments in the helical state can be calculated exactly in terms of the 'cooperativity parameter' σ and ϵ.

It is equally well known [12] that, when a polymer chain is exposed to an attractive planar surface, there exists a critical adsorption temperature T_{c} above which the fraction ϕ of polymer segments adsorbed to the surface is zero. In the exactly solvable model [12] of adsorption of a flexible chain to a surface, the polymer chain is assumed to be a Gaussian chain of N Kuhn segments, connected contiguously with step length l. The short-range attraction between the surface and polymer segments is parameterized by a pseudo-potential $Cl\delta(z)$ where z is the direction perpendicular to the surface and $C = (T - T_{\mathrm{c}})/T_{\mathrm{c}}$. Exact mathematical expressions [12] are known for the partition sums, both full and constrained such as fixing the chain ends at the surface, in terms of N and C.

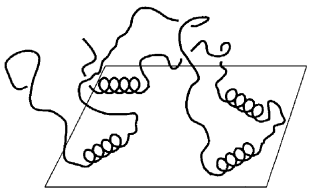

Figure 9. Sketch of the model.

We model the coupling between the helix–coil transition and adsorption as follows. To begin with, the polymer chain is taken (in the absence of any helix formation) to be a Gaussian chain of N Kuhn segments and step length l. Then each segment can be either in the coil state or in the helical state. Therefore, a typical configuration is a continuous connection of strings of helical segments and strings of coil segments. Let η be the probability to initiate a string of helical segments. η is the cooperativity parameter σ ($\eta = \sigma$). Let $-\epsilon$ be the free energy per segment in the helical state relative to that in the coil state. Now the chain is exposed to a planar interface. The interaction between the interface and segments in the coil state is $Cl\delta(z)$. In view of empirical evidence for preferential adsorption of helical segments (over coil segments) at the air-water interface, we assume that all helical segments are at the interface. The model of the polymer addressed here (figure 9) consists of helical strings in contact with the surface and loops of coil segments (away from the surface) subjected to interaction with the surface described above. Whether the chain ends are in the coil state or in the helix state is irrelevant in the thermodynamic limit. The excluded volume and electrostatic interactions among various segments of experimental systems are ignored in this model and the chain obeys Gaussian statistics if there are no helical segments and the surface.

It is particularly convenient to employ the propagator formalism [14] of helix–coil transition in the exact calculation of the partition sum for this model as a function N, ϵ, η and C. Representing a helical string of m segments to be a rod of length ml embedded on the surface with end-to-end distance $\mathbf{R}_\parallel - \mathbf{X}_\parallel$, its propagator is

$$g_{\text{rod}}(\mathbf{R}_\parallel - \mathbf{X}_\parallel) = \frac{\eta e^{\epsilon m}}{2\pi \mid \mathbf{R}_\parallel - \mathbf{X}_\parallel \mid} \delta^{(2)}(\mid \mathbf{R}_\parallel - \mathbf{X}_\parallel \mid - ml). \tag{22}$$

The propagator for a loop of n segments with its ends at $\mathbf{R}_\parallel$ and $\mathbf{X}_\parallel$ is [12]

$$g_{\text{loop}}(\mathbf{R}, \mathbf{X}; n) = 2\left[\frac{3}{2\pi n l^2}\right]^{3/2} [1 - \sqrt{\pi}\Gamma\, \mathrm{e}^{\Gamma^2} erfc(\Gamma)] \exp\left[-\frac{3(\mathbf{R}_\parallel - \mathbf{X}_\parallel)^2}{2nl^2}\right] \tag{23}$$

with $\Gamma = C\sqrt{6n}$. The full propagator $G(\mathbf{R}_\parallel, \mathbf{0}; N)$ for the chain with the end-to-end distance $\mathbf{R}_\parallel$ can be calculated by summing over all possible distributions of segments into helical and coil states with their appropriate weights. The exact summation is shown diagrammatically in figure 10. As usual, the summation is facilitated by defining the Fourier–Laplace transform,

$$\tilde{G}(\mathbf{k}_\parallel; t) = \int_0^\infty \mathrm{d}N \exp(-Nt) \int \frac{\mathrm{d}\mathbf{R}_\parallel}{(2\pi)^2} \exp(-i\,\mathbf{k}_\parallel \cdot \mathbf{R}_\parallel) G(\mathbf{R}_\parallel, \mathbf{0}; N) \tag{24}$$

Figure 10. Diagrammatic representation of the propagators for the helix–coil transition.

for the various propagators. In figure 10, straight lines and wiggly lines represent $\tilde{g}_{\rm rod}$ and $\tilde{g}_{\rm loop}$ respectively, and

$$\tilde{G}(\mathbf{k}_{\|};t) = [\tilde{g}_{\rm rod}^{-1}(\mathbf{k}_{\|};t) - \tilde{g}_{\rm loop}(\mathbf{k}_{\|};t)]^{-1}. \tag{25}$$

The partition sum Z is the sum over all possible configurations of the chain, $\int \mathrm{d}\mathbf{R}_{\|} G(\mathbf{R}_{\|}, \mathbf{0}; N)$, given by

$$Z = 4\pi^2 A \int_{\gamma - i\infty}^{\gamma + i\infty} \frac{\mathrm{d}t}{2\pi i} \exp(Nt)\tilde{G}(0;t), \tag{26}$$

where A is the area of the surface and $\tilde{G}(0;t)$ follows from eqs (22)–(25) as

$$\tilde{G}(0;t) = \frac{\eta(\sqrt{t} + \sqrt{6}C)}{t^{3/2} + \sqrt{6}Ct - \epsilon t^{1/2} - \epsilon\sqrt{6}C - \eta\sqrt{6}/l}. \tag{27}$$

The fraction θ of segments in the helix state and the fraction ϕ of segments in the coil state at the surface are calculated from

$$\theta = \frac{1}{N}\frac{\partial \ln(Z)}{\partial \epsilon}; \quad \phi = -\frac{1}{N}\frac{\partial \ln(Z)}{\partial C}. \tag{28}$$

Exact results for θ and ϕ follow from eq. (28). We illustrate the results for two cases, $\eta = 1$ and $\eta \to 0$. Figures 11a and 11b give the dependence of θ on ϵ for attractive ($C < 0$) and repulsive ($C > 0$) surfaces, respectively. When C is very small, we recover the typical sigmoidal 'helix–coil' transition curve with dominance of helix segments and coil segments respectively for positive and negative ϵ values. For attractive surfaces, when $-C$ increases, attraction of coil segments to the surface begins to interfere with the formation of helical segments. For $-10 < C < -1$, θ decreases abruptly with an increase of $-C$ even for large positive values of ϵ. For $C < -10$, the polymer is almost completely absorbed onto the surface and it is energetically more favorable for the segments to leave the helical conformation and adsorb onto the surface as segments of the coil state. Therefore, adsorption dominates over helix–coil transition. We describe below the nature of the adsorption transition under these circumstances by considering the limit $\eta \to 0$.

For repulsive surfaces (figure 11b), the usual sigmoidal shape of θ from helix to coil conformations as ϵ is decreased from positive to negative values is recovered for small values of $C \approx 10^{-3}$. As the strength of repulsion between the surface and coil segments increases, entropic stabilization of large loops competes against the formation of helical segments. This is found to lead to a true thermodynamic phase transition for the helix–coil transition. θ is zero for $\epsilon \leq \epsilon_0 = -\eta C$. At ϵ_0 there is a sharp change of θ which gets sharper as the surface becomes more repulsive. In spite of the very sharp appearance of θ versus ϵ for higher C values, the transition is a second order phase transition and $\lim_{\epsilon \to \epsilon_0^+} \partial\theta/\partial\epsilon = 2(C^4/\eta^2)$. For repulsive surfaces, $\epsilon = -(\eta/C)$ is a line of critical points.

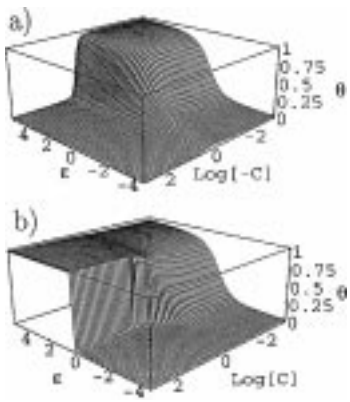

Figure 11. Rod fraction: (a) attractive surface, (b) repulsive surface.

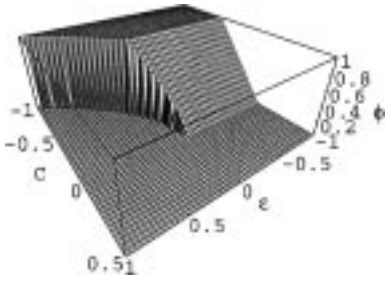

Figure 12. Fraction of coil segments in contact with the surface.

The modification of the adsorption transition by the presence of helical segments can be determined exactly by considering the limit $\eta \to 0$ and taking the chain ends in the coil state (figure 12). When $\epsilon < 0$ (preference of coil over helical segments) ϕ versus C is the usual adsorption behavior of a flexible chain, with ϕ vanishing at $C = 0$ (second order phase transition). A line of second order phase transitions is obtained for $\epsilon < 0$. As ϵ increases with increasing population of helical segments, the adsorption temperature is lowered and ϕ is nonzero only for $6C^2 > \epsilon$. Also the nature of the adsorption transition changes. These are consequences of the competition between helix formation which minimizes the free energy related to the ϵ parameter and adsorption of coil segments which minimizes the free energy at the surface. Both situations cannot take place simultaneously and consequently the phase transition becomes first order, as seen in the discontinuity of ϕ. $6C^2 = \epsilon$ is a line of first order phase transitions (for $\epsilon > 0$) meeting at $\epsilon = 0 = C$ with the line of second order transitions (for $\epsilon < 0$). Therefore, the point $\eta \to 0$, $\epsilon = 0$, $C = 0$ is a tricritical point for infinitely long polymer chains.

We conclude that adsorption of a polymer chain which can undergo the helix–coil conformational transition in bulk shows a rich phase diagram, with the non-thermodynamic helix-coil transition getting promoted to a second order phase transition and the adsorption transition becomes first order. The Gaussian statistics for coil segments needs to be modified in any quantitative comparison with experimental systems, to account for electrostatic, hydrophobic and other interactions.

4. Model for chromosomal condensation

We introduce a model to describe the distribution of chromatin loops described in figure 3. Since the typical lengths of various loops are much longer than the persistence length, we represent the chromatin fiber as a continuous curve and the probability distribution function, $g_0(\mathbf{R}, \mathbf{R}'; N)$ for the chain of N segments to have the ends at $\mathbf{R}$ and $\mathbf{R}'$ is given by the Edwards path integral

$$g_0(\mathbf{R}, \mathbf{R}'; N) = \int_{\mathbf{R}(0)=\mathbf{R}'}^{\mathbf{R}(L)=\mathbf{R}} \mathcal{D}[R(s)] \exp\left\{ -\frac{3}{2l} \int_0^L \mathrm{d}s \left(\frac{\partial \mathbf{R}(s)}{\partial s} \right)^2 \right\}. \tag{29}$$

Here $L = Nl$ is the contour length, l is the Kuhn length, and $\mathbf{R}(s)$ is the position vector of the arc length variable $s(0 \leq s \leq L)$. In addition we assume that there are rigid rod-like anchoring complexes each of length l which complex with the chromatin fiber in various possible configurations shown in figure 13. It is assumed that anchoring complexes are present only in conjunction with loops and bridges of chromatin.

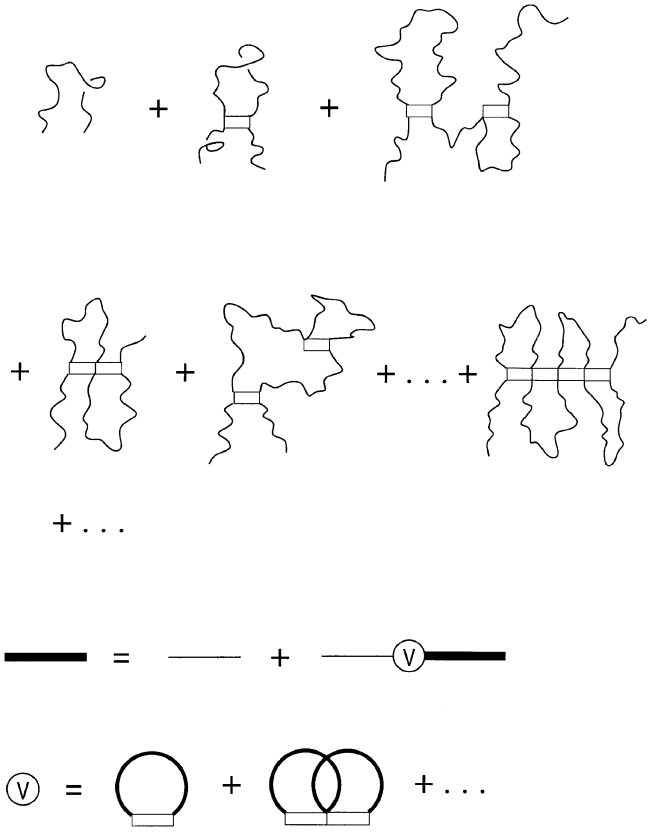

Figure 13. Sample configurations in chromosomal condensation and their diagrammatic summation.

Let the probability distribution function $\gamma(\mathbf{R}-\mathbf{R}')$ for an anchoring complex with end-to-end distance $\mathbf{R}-\mathbf{R}'$, to be

$$\gamma(\mathbf{R}-\mathbf{R}') = \frac{\eta e^{\epsilon}}{4\pi|\,\mathbf{R}-\mathbf{R}'|^2}\,\delta(|\,\mathbf{R}-\mathbf{R}'|-l\,), \tag{30}$$

where $-\epsilon$ is the free energy associated with the formation of the anchoring complex. η is a parameter denoting the probability of nucleating an anchoring complex. Employing the propagator formalism, all configurations in figure 13 can be summed and the partition sum is expressed in terms of the parameters N, ϵ and η of the model. Using the Fourier–Laplace transform of g_0, the propagator for any flexible portion of the chain is

$$\tilde{g}_0(\mathbf{k},E) = \int_0^{\infty} \mathrm{d}N\,\mathrm{e}^{-EN}\int \mathrm{d}^3R\,\mathrm{e}^{-i\mathbf{k}\cdot\mathbf{R}}g_0(\mathbf{R},\mathbf{0};N) = \frac{1}{((k^2\ell^2/6)+E)}. \tag{31}$$

Using the Fourier transform of γ, the propagator for an anchoring complex is

$$\begin{aligned}\tilde{\gamma}(\mathbf{k}) &= \int \mathrm{d}^3\,R\,\mathrm{e}^{-i\mathbf{k}\cdot\mathbf{R}}\gamma(\mathbf{R})\\ &= \frac{\eta\,\mathrm{e}^{\epsilon}}{kl}\sin(kl).\end{aligned} \tag{32}$$

Using these propagators, the various graphs in figure 13 can readily be calculated. The propagator $\tilde{G}(\mathbf{k},E)$ for the full probability distribution function, by summing all terms in figure 13 is given exactly by (see ref. [14] for details)

$$\tilde{G}(\mathbf{k},E) = \tilde{g}_0(\mathbf{k},E) + \tilde{g}_0(\mathbf{k},E)V(\mathbf{k},E)\tilde{G}(k,E), \tag{33}$$

where

$$V(\mathbf{k},E) = \eta\sum_{\mu=1}^{\infty}\frac{(\mathcal{L}\,\mathrm{e}^{\epsilon})^{\mu}}{\mu kl}\sin(\mu kl)$$

with

$$\mathcal{L} = l^3\int\frac{\mathrm{d}^3j}{(2\pi)^3}\,\tilde{G}(\,\mathbf{j},E). \tag{34}$$

Equation (33) is represented graphically in figure 13 where thick line is the full propagator $\tilde{G}$ and thin line is the bare propagator g_0. The above exact expressions for the model introduced here allow for the occurrence of multiple nuclei involving anchoring complexes. If only one nucleus is allowed to form the chromosomal axis then $\mathcal{L}$ is given simply by

$$\mathcal{L} = l^3\int\frac{\mathrm{d}^3j}{(2\pi)^3}\,\tilde{g}_0(\,\mathbf{j},E). \tag{35}$$

It follows from the above equations that

$$\tilde{G}(\mathbf{0},E) = \frac{1}{E-V(\mathbf{0},E)} \tag{36}$$

and the partition sum Z_N is the inverse Laplace transform of $\tilde{G}(\mathbf{0}, E)$,

$$Z_N = \int \frac{\mathrm{d}E}{2\pi i}\, \mathrm{e}^{EN}\, \tilde{G}(0, E). \tag{37}$$

All thermodynamic quantities such as the free energy of the complex, average length of the chromosomal axis, average radial extension of loops, the radius of gyration of the complex, etc., follow from Z_N as functions of the parameters N, ϵ and η of the model. One of the key results of this calculation is that the size of the complex is independent of the length of the chromatin fiber (N) in the condensed state and is proportional to $\sqrt{N}$ in the uncondensed state. The extent of compactification is determined by the values of the parameters. The details of the calculational results and their analysis will be presented in a future publication.

5. Thermodynamics of polyelectrolytes in crowded environments

A theoretical description of the collective properties of polyelectrolyte solutions is a challenge. Consider a system of n polyelectrolyte chains each of N segments, n_c counterions, n_γ ions of species γ from dissolved salt and n_s solvent molecules in volume Ω. Each of the $N\alpha$ segments of a chain carries a charge of eZ_p where e is the electronic charge and α is the degree of ionization per chain. Assuming that the total charge $N\alpha eZ_p$ of the chain is uniformly distributed along the chain backbone, the excluded volume interaction $V_0(\mathbf{r})$ between polymer segments separated by a distance $\mathbf{r}$ is modeled by the sum of a delta function pseudopotential of strength w and the Coulomb potential of strength $Z_p^2\alpha^2 l_\mathrm{B}\, k_\mathrm{B}\, T$,

$$\frac{V_0(\mathbf{r})}{k_\mathrm{B}T} = w\delta(\mathbf{r}) + Z_p^2\alpha^2 l_\mathrm{B}\frac{1}{r}, \tag{38}$$

where r is $|\mathbf{r}|$. The interaction between ith ion of charge eZ_i and jth ion of charge eZ_j is taken to be $(Z_i Z_j\, l_\mathrm{B})$ where r is the distance of separation between these ions. The excluded volume interaction between a polymer segment and a solvent molecule is modeled by a delta function pseudopotential of strength w_{ps}. Similarly w_{ss} is the strength of the excluded volume interaction between two solvent molecules.

What is the equation of state for such a system? A correct formulation of this problem must address the following double screening [15]. It is well known that the Coulomb interaction between any two charges separated by a distance r in an electrically neutral system is screened by the presence of other randomly distributed charges to the familiar Debye–Hückel form [16],

$$\frac{1}{r} \longrightarrow \frac{1}{r}\exp(-\kappa r), \tag{39}$$

where the Debye length κ^{-1} depends on the concentration of randomly distributed ions. ($\kappa^2 \sim c_s$, where c_s is the salt concentration). In the case of polyelectrolytes, many charged ions are topologically correlated by chain connectivity. This topological correlation alters the form of the Debye–Hückel potential, which is purely repulsive between similarly charged ions. To emphasize the significance of topological correlation, we must mention that short-range potential interaction between any two polymer segments in a solution of

neutral polymers is screened by other polymer segments, which are entropically correlated, to the Edwards form [17],

$$w\delta(r) \longrightarrow w\left[\delta(r) - \frac{1}{4\pi r\xi^2}\exp\left(-\frac{r}{\xi}\right)\right], \tag{40}$$

where the Edwards length ξ depends on w and the polymer concentration c. For example, ξ is proportional to $c^{-(3/4)}$ in semidilute solutions, where the chain obeys the self-avoiding walk statistics in infinitely dilute solutions. Thus, for the case of polyelectrolyte solutions, it is necessary to account for both the electrostatic and topological screenings in deriving the free energy of the system. The net effect of these screenings is that the effective interaction V_{eff} between two similarly charged monomers can be attractive at intermediate large distances of separation. The magnitude and range of this attraction between similarly charged monomers has been derived [15, 18] for solutions of many charged flexible polyelectrolytes, charged spheres and charged cylinders in terms of concentrations of the macroions and small salt ions. The qualitative explanation of this attraction at intermediate distances is the following. Between similarly charged monomers, the electrostatic interaction is purely repulsive with its range κ^{-1} given by the salt concentration c_s. The Edwards screening leads to an effective interaction between segments which is attractive with its range ξ given by the polymer concentration c. A superposition of these two terms with different ranges can lead to attraction at intermediate distances for favorable values of κ^{-1} and ξ. In general, provided the salt concentration is low enough, the strength and range of attraction increases and decreases, respectively, if the polyelectrolyte concentration is increased. Typically the strength of the attraction is about $10^{-2}k_{\text{B}}T$ per pair of segments and consequently can be very substantial between chains ($N \sim 10^3$). The range is about $\simeq 50\,\text{Å}$ for flexible polyelectrolytes allowing the formation of loose aggregates (see refs. [15] and [18] for details). As an example, the effective interaction per a pair of segments (of linear dimension l) belonging to two rod-like polymers (diameter $= 0.1l$, $l_{\text{B}} = 0.8l$, length $= 1000l$) at a volume fraction of 0.05 is given in figure 14. V_{eff} is the effective interaction potential between a pair of segments in units of $k_{\text{B}}T$ and r is the distance between the segments in units of l. In figure 14, the values of κ are: 0.6 ($\triangle$), 0.8 ($\square$), 1.0 ($\circ$), 2.0 ($\diamond$), and 4.0 (∇).

Thus a key result of our description of thermodynamics of charged polymers is the theorem that similarly charged monomers can attract if the similarly charged mediating objects are sufficiently topologically correlated (by stringing charges together into a

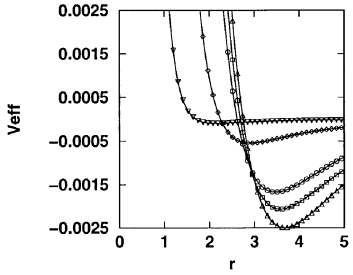

Figure 14. Effective potential vs. distance between segments of similarly charged rods.

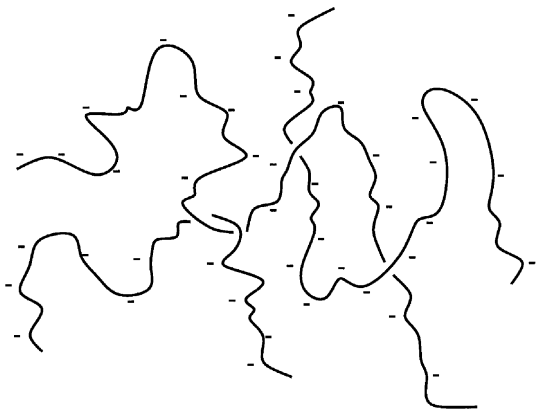

Figure 15. Several interpenetrating polyelectrolyte chains.

polyelectrolyte or wrapping charges on surfaces of planes, spheres, cylinders, etc.) and are present in sufficiently large concentrations for low enough salt concentrations.

This effect, in turn, is believed to play a crucial role in the manifestation of various temporal biological functions. In addition this collective effect leads to an enhanced stabilization of the isotropic phase against the formation of the nematic phase in a solution of charged rods such as the microtubules and short DNA molecules. The reader is referred to ref. [18] for details.

6. Collective dynamics of polyelectrolytes

Consider a solution containing n linear polymer chains each of contour length L bearing electric charges uniformly placed along their backbones, as illustrated in the cartoon of figure 15. The neutralizing counterions and any added salt are also present in the solution. How do the polymer chains diffuse around in the absence of any external fields?

The general features of the dynamical properties of polyelectrolyte solutions are dramatically different from those of neutral polymers, as richly documented [19–22] in the literature. As one example, we consider the typical dynamic light scattering data exhibited by solutions of synthetic polyelectrolytes, proteins, DNA, and other charged macromolecules. In dynamic light scattering, the diffusion coefficient D is obtained by fitting the dynamic structure factor $S(k,t)$ to an exponential in k^2t,

$$S(k,t) = \langle \rho_k(t)\rho_{-k}(0)\rangle \sim \exp(-Dk^2\, t), \tag{41}$$

where k is the scattering wave vector and $\rho_k(t)$ is the Fourier transform of the local segment density,

$$\rho_{\mathbf{k}}(t) = \sum_{\alpha=1}^{n}\sum_{i=1}^{N} \exp(i\,\mathbf{k}\cdot\mathbf{R}_{\alpha i}(t)), \tag{42}$$

with $\mathbf{R}_{\alpha i}(t)$ being the position vector of the ith segment of chain α at time t. The diffusion coefficient D measured in dilute solutions of polyelectrolytes with high salt concentrations (sufficient to screen out any long-range electrostatic interactions between segments) is

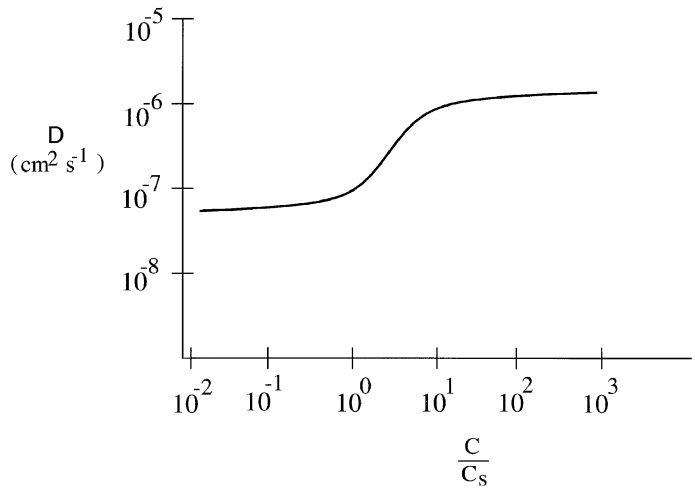

Figure 16. Dependence of the fast diffusion coefficient on c/c_s.

comparable to that for neutral polymers with the same molecular weight. This value of D is in agreement with expectations based on the Stokes–Einstein law,

$$D = \frac{k_B T}{6\pi\eta_0 R_g}, \tag{43}$$

where R_g is the radius of gyration of the polymer and η_0 is the zero-shear-rate viscosity of the solvent. As the salt concentration is lowered, the electrostatic interaction among polymer segments is less screened and thus the polymer chain is more swollen than in higher salt concentrations. Therefore we expect from the Stokes–Einstein law that D decreases with lowering the concentration of added salt but keeping the polyelectrolyte concentration very low. In fact, D increases by at least an order of magnitude and eventually approaches a value in 'salt-free' solutions, which is independent of molecular weight of the polyelectrolyte and comparable to that of a monomer. Furthermore, in 'salt-free' solutions, the value of D is independent of polyelectrolyte concentration over a range of three orders of magnitude in c. These observations are sketched in figure 16 and details are found in refs. [22], [23]. Summarising these observations, the asymptotic results of D (called the 'fast' diffusion coefficient) are,

$$D \sim \begin{cases} N^{-3/5}, & c/c_s \ll 1 \\ c^0 N^0, & c/c_s \gg 1. \end{cases} \tag{44}$$

It must be pointed out that while the high value of D is observed at $c/c_s \gg 1$, another mode called 'slow mode' appears in the dynamic light scattering with a diffusion coefficient D_s three orders of magnitude smaller than D. For a discussion of this slow mode see refs [23], [24].

An adequate description of dynamics of polyelectrolyte solutions must include a consideration of the following features: (a) electrostatic screening by small ions, (b) excluded volume screening due to chain connectivity and its coupling to electrostatic screening, (c) hydrodynamic screening, i.e., modification of the long-range Oseen interaction by the

presence of polymer chains, (d) electrostatic coupling between polyelectrolytes and their counterions, and (e) entanglement effects. The results of figure 16 are in the concentration regime where the entanglement effects are weak. We have derived a general theory [24] of dynamics of polyelectrolyte solutions accounting for the above mentioned features. The essentials of this theory in the context of figure 16 are discussed below.

The continuity equation for the monomer density is

$$\frac{\partial \rho(\mathbf{r})}{\partial t} = -\nabla \cdot \mathbf{J}(\mathbf{r}), \tag{45}$$

where the current $\mathbf{J}(\mathbf{r})$ is given by

$$\mathbf{J}(\mathbf{r}) = -D_c \nabla \rho + \rho \mu \mathbf{E}_i. \tag{46}$$

The first term is the usual 'diffusive' term proportional to the gradient of the chemical potential with D_c being the cooperative diffusion coefficient. Based on the coupling among three long-ranged interactions (electrostatic, chain connectivity, and hydrodynamic), D_c can be derived [24] to obey the results,

$$D_c \sim \begin{cases} N^{-\nu}, & c \ll c^* \\ c^{\nu/(3\nu-1)}, & c \gg c^* \end{cases} \tag{47}$$

where ν is the radius of gyration exponent, $R_g \sim N^{\nu}$ and $c^* \sim N^{1-3\nu}$ is the overlap concentration. As noted above $\nu = 1$ and $3/5$ in the limits of low salt and high salt, respectively. With only the first term of eq. (46), the above results are the standard results for neutral polymers [25].

The crucial aspect of collective dynamics of polyelectrolytes is the presence of the second term in eq. (46). This 'convective' term arises from the coupling between polymer segments and their counterions, where μ is the electrophoretic mobility of segments and $\mathbf{E}_i$ is the electric field induced on the segments by the counterions. $\mu \mathbf{E}_i$ is the velocity of segments created by the electrostatic coupling between segments and their counterions. The electrophoretic mobility has been derived [24] to be for $c \ll c^*$

$$\mu \sim \begin{cases} N^0, & \text{low salt,} \\ N^0 \kappa^{-(2/3)}, & \text{high salt,} \end{cases} \tag{48}$$

and for $c \gg c^*$

$$\mu \sim c^{-(1-\nu)/(3\nu-1)}. \tag{49}$$

Substituting eq. (46) into eq. (45) we get

$$\frac{\partial \rho(\mathbf{r})}{\partial t} = = D_c \nabla^2 \rho(\mathbf{r}) - \rho \mu \nabla \cdot \mathbf{E}_i. \tag{50}$$

Using the Poisson equation,

$$\nabla \cdot \mathbf{E}_i = \frac{4\pi}{\epsilon} (z_p e \rho + z_c e \rho_c + \cdots), \tag{51}$$

where ϵ is the effective dielectric constant of the solution, $z_p e$ is the electric charge of a polymer segment, $z_c e$ is the electric charge of the counterion corresponding to the

segment and ρ_c is the concentration of the counterions. The dotted terms represent factors corresponding to ions arising from added salt. Writing the continuity equation for the counterion concentration,

$$\frac{\partial \rho_c(\mathbf{r})}{\partial t} = = D'\nabla^2 \rho_c(\mathbf{r}) - \rho_c \mu_c \frac{4\pi}{\epsilon}(z_p e\rho + z_c e\rho_c + \cdots), \tag{52}$$

where D' is the diffusion coefficient of the counterion and $\mu_c = z_c eD'/k_B T$ is the electrophoretic mobility of the counterion. If we make the reasonable assumption that counterions relax much faster than the polyelectrolyte chains, the above equations simplify in the linear response regime to

$$\frac{\partial \rho_{\mathbf{k}}(t)}{\partial t} = -\left[D_c + \frac{4\pi}{\epsilon}\frac{z_p e\mu c}{\kappa^2}\right]k^2 \rho_{\mathbf{k}}. \tag{53}$$

In obtaining this result, $k \to 0$ limit is taken and the Debye–Hückel relation, $\kappa^2 = (4\pi/\epsilon k_B T) z_c^2 e^2 \rho_c$, is employed. If salt ions are present, eq. (53) is still valid except that κ^2 is given by the Debye–Hückel theory including the salt ions. It follows from eq. (53) that

$$\langle \rho_{\mathbf{k}}(t)\rho_{-\mathbf{k}}(0)\rangle \sim \exp(-D_{\text{coupled}}\, k^2 t), \tag{54}$$

with

$$D_{\text{coupled}} = \left[D_c + \frac{4\pi}{\epsilon}\frac{z_p e\mu c}{\kappa^2}\right], \tag{55}$$

where the first and second terms respectively are due to the diffusive part and the counterion-polyelectrolyte coupling. In 'salt-free' solutions $\kappa^2 \sim \rho_c \sim c$ and $\mu \sim N^0 c^0$, so the second term is a constant independent of N and c. By putting the numerical values of various coefficients in eq. (55) using the results of ref. [24], the second term can be shown to dominate the first term in 'salt-free' solutions. Thus the observed high diffusion coefficient independent of N and c in salt-free solutions is due to the electrostatic coupling between the counterions and the polyelectrolyte. The rapidly diffusing small counterions are dragging the gigantic polyelectrolyte with them in the weak salt limit. On the other hand, if the salt concentration is high (κ large), the first term dominates the right hand side of eq. (55). These are the essential results of figure 16.

7. Polymer transport through pores

In biological environments within cells polymers are partitioned into various compartments and they are transported from one compartment into another using regulatory signaling pathways. For example *m*-RNA (containing information for protein synthesis) is transferred from the cell nucleus to the cytoplasm through the nuclear pore. The nuclear pore itself is a self-assembled complex of many protein molecules and the channels in the nuclear pore are smaller or comparable to the size of the macromolecules. How does a polymer chain go through the nuclear pore? In general this transport is a difficult process requiring very long times and consequently ratchet potentials associated with appropriate decoration of the nuclear pore are provided in nature.

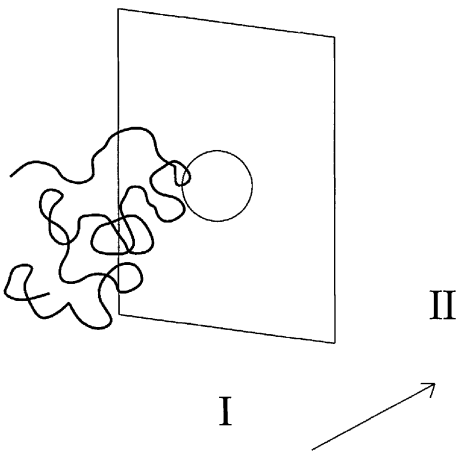

Figure 17. Escape of a chain through a hole.

To address this general question, let us imagine a long polymer of N segments in region I to be transported into region II. Let these regions be divided by a partition which is taken to be an infinite two-dimensional sheet with a hole in the middle to allow the passage of the chain (figure 17). Except for this hole, the sheet is a hard wall for polymer segments. Let the chemical potentials of the polymer segment be μ_1 and μ_2, respectively in regions I and II. The chain is assumed to obey the same chain statistics in both regions and the actual differences in chain statistics in these regions are assumed to be included in the chemical potential difference $\Delta\mu = \mu_2 - \mu_1$.

The Monte Carlo simulations of this model reveal that there are three stages: (i) a very slow process of placing an initial monomer at the entrance of the hole, (ii) attempts to make a stable nucleus of enough monomers in region II, and (iii) the eventual slippage of the chain into region II, when $\Delta\mu < 0$. The durations of these stages vary depending on the details of the various potentials and parameters. As a specific example, let us consider the exactly solvable model corresponding to the third stage. Let m segments be present in region II and $N - m$ segments be in region I (figure 18) and the size of the hole is small enough to allow only one segment (hairpins are not allowed). The free energy of this polymer configuration is obtained in the following way. The partition sum Z_m for a polymer chain of m segments in a semi-infinite space with a hard wall and one end permanently anchored at the center of the wall is given by

$$Z_m \sim m^{\gamma'-1}, \tag{56}$$

where $\gamma' = 0.5, 0.69$, and 1 for Gaussian, self-avoiding, and rod-like chains, respectively. Therefore the free energy F_m associated with this configuration is

$$\frac{F_m}{k_B T} = (1-\gamma')\ln[m(N-m)] + m\frac{\Delta\mu}{k_B T}, \tag{57}$$

where the unnecessary constant terms are ignored. F_m exhibits a free energy barrier as a function of m. Following the usual arguments of the nucleation theory, the transport of the

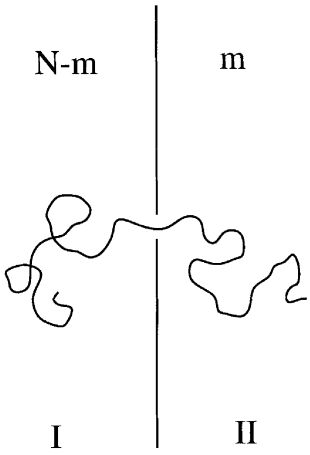

Figure 18. Polymer escape in transition.

chain through the free energy barrier is described by

$$\frac{\partial W_m(t)}{\partial t} = \frac{\partial}{\partial m}\left[\frac{D_m}{k_B T}\frac{\partial F_m}{\partial m} W_m(t) + D_m \frac{\partial}{\partial m} W_m(t)\right], \tag{58}$$

where W_m is the probability of finding a nucleus of m segments in region II and D_m is the rate constant for the formation of a nucleus with $m+1$ segments from a nucleus with m segments. Since every monomer is transported locally at the hole, we take D_m to be inversely proportional to the segmental friction coefficient at the hole and independent of N. The mean first passage time τ for the process described by eq. (58), i.e., the averasge time required by the chain, having already placed at least one segment in region II, to go from region I to region II is

$$\tau = \frac{1}{D_m}\int_0^N \mathrm{d}m_1 \exp\left(\frac{F_{m_1}}{k_B T}\right)\int_0^{m_1} \mathrm{d}m_2 \exp\left(-\frac{F_{m_2}}{k_B T}\right). \tag{59}$$

Substituting eq. (58) in eq. (59), τ for long Gaussian chains is given by, for symmetric barriers

$$D_m \tau = \frac{\pi^2}{16} N^2, \quad \Delta\mu = 0, \tag{60}$$

and for asymmetric barriers

$$D_m \tau \sim \begin{cases} \frac{k_B T}{\Delta\mu} N, & \Delta\mu \ll 0 \\ \left(\frac{k_B T}{\Delta\mu}\right)^2 \exp(N\frac{\Delta\mu}{k_B T}), & \Delta\mu \gg 0. \end{cases} \tag{61}$$

The general results are given in figure 19 where τ (in units of $1/D_m$) is plotted against N for different values of $\Delta\mu/k_B T$. As is clearly seen, the chemical potential difference between regions I and II controls significantly the value of the escape time τ. Furthermore it must be pointed out that τ is proportional to N when the escape is in the direction of

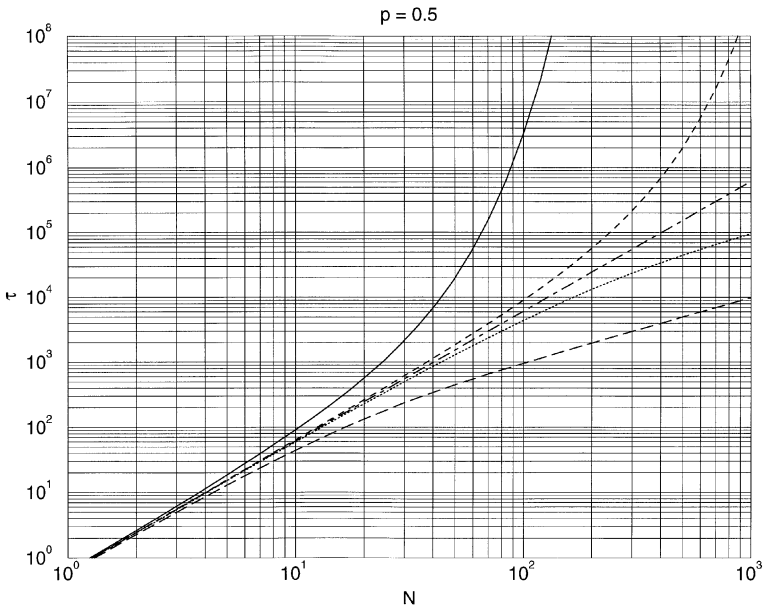

Figure 19. Dependence of escape time τ on N for different values of $\Delta\mu/k_BT$ $(-0.1, -0.01, 0, 0.01, 0.1)$. τ increases with $\Delta\mu/k_BT$ as given by eqs. (60)–(61).

the favorable chemical potential gradient and not to N^2 as has previously been claimed in the literature [26]. Our conclusion is in agreement with experimental findings [27]. The results given in eqs. (60), (61) and figure 19 are rather insensitive to the value of the exponent γ' of eq. (56).

Acknowledgement

The author was pleased to participate in the Golden Jubilee of the Raman Research Institute and is grateful to the organizers for this opportunity. Acknowledgment is made to the NSF for Grant DMR 9625485 and the Materials Research Science and Engineering Center at the University of Massachusetts. The author is pleased to thank G A Carri, C Y Kong, R Mondescu, V Prabhu, and P Welch for stimulating discussions and help with figures.

References

[1] B Alberts, D Bray, J Lewis, M Raff, K Roberts and J D Watson, *The Molecular Biology of the Cell*, 2nd ed. (Garland Publ. Co., New York, 1994)
[2] H Lodish, D Baltimore, A Berk, S L Zipursky, P Matsudaira and J Darnell, *Molecular Cell Biology* (W H Freeman and Co., New York, 1997)
[3] M Muthukumar, *Current Opinion in Colloid Interface Science* **3**, 48 (1998)
[4] S F Edwards, *Proc. Phys. Soc. London* **85**, 613 (1965)
[5] M Muthukumar, *J. Chem. Phys.* **103**, 4723 (1995)
[6] M Beer, M Schmidt and M Muthukumar, *Macromolecules* **30**, 8375 (1997)

[7] C Y Kong and M Muthukumar, *J. Chem. Phys.* **109**, 1522 (1998)
[8] F von Goeler and M Muthukumar, *J. Chem. Phys.* **100**, 7796 (1994)
[9] D Srivastava and M Muthukumar, *Macromolecules* **27**, 1461 (1994)
[10] M Muthukumar, *Computational Materials Science* **4**, 370 (1995)
[11] D Poland and H A Scheraga, *Theory of Helix-Coil Transitions in Biopolymers. Statistical Mechanical Theory of Order-Disorder Transitions in Biological Macromolecules*, (Academic Press, New York, 1970)
[12] E Eisenriegler, *Polymers near Surfaces* (World Scientific, Singapore, 1993)
[13] G A Carri and M Muthukumar, *Phys. Rev. Lett.* (in press)
[14] M Muthukumar, *J. Chem. Phys.* **104**, 691 (1996)
[15] M Muthukumar, *J. Chem. Phys.* **105**, 5183 (1996)
[16] P Debye and E Hückel, *Phys. Z.* **24**, 185 (1923)
[17] S F Edwards, *Proc. Phys. Soc.* **88**, 265 (1966)
[18] G A Carri and M Muthukumar, *J. Chem. Phys.* (in press)
[19] K S Schmitz, *Macroions in Solution and Colloid Suspension* (VCH, New York, 1993)
[20] K S Schmitz, *An Introduction to Dynamic Light Scattering by Macromolecules* (Academic, New York, 1990)
[21] H Dautzenberg, W Jaeger, J Kötz, B Philipp, Ch. Seidel and D Stscherbina, *Polyelectrolytes* (Hanser, New York, 1994)
[22] S Förster and M Schmidt, *Adv. Polym. Sci.* **120**, 51 (1995)
[23] M Sedlak, *J. Chem. Phys.* **105**, 10123 (1996)
[24] M Muthukumar, *J. Chem. Phys.* **107**, 2619 (1997)
[25] M Doi and S F Edwards, *The Theory of Polymer Dynamics* (Clarendon, Oxford, 1986)
[26] W Sung and P J Park, *Phys. Rev. Lett.* **77**, 783 (1996)
[27] J J Kasianowicz, E Brandin, D Branton and D W Deamer, *Proc. Natl. Acad. Sci. USA* **93**, 13770 (1996)